# Inverse-Designed Aperiodic Multilayer Graphene-Based Perfect Absorbers for Mid-IR Applications: Precision Tunability, Electrical Switchability, and Angular Robustness

## Supplemental Material

Masoumeh Nazari, Yaser M. Banad, and Sarah Sharif *

*The School of Electrical and Computer Engineering, University of Oklahoma, Norman, OK 73019, USA*

** Corresponding Author email: s.sh@ou.edu*

### Supplemental Material S1: Simulation Parameters and Computational Methodology

The simulations were carried out using the finite-difference time-domain (FDTD) method. FDTD was employed for full-wave electromagnetic analysis, field distribution, angular performance, and switchability simulations, while TMM was used for fast spectral calculations and initial design validation. Graphene was modeled using the Transition Boundary Condition (TBC) approach rather than as a volumetric layer, allowing for an accurate representation of its optical behavior while significantly reducing computational complexity. The optical conductivity of graphene was defined using the Kubo formula**,** accounting for both intraband and interband transitions.

The simulation domain was bounded by periodic boundary conditions in the x- and y-directions to emulate an infinite structure, while Perfectly Matched Layers (PMLs) were applied in the z-direction to absorb outgoing waves. A plane wave source was used, incident from the top along the z-axis, implemented via a Port boundary condition with excitation enabled. The simulations were conducted over the 3–5 μm wavelength range**.**

To ensure numerical stability and accurate field resolution—especially near the ultrathin graphene layers—an Extremely Fine, physics-controlled mesh was employed. Additional mesh refinement was applied along the z-direction to resolve sub-wavelength layer thicknesses and steep field gradients.

For structural optimization, we used a micro-genetic algorithm to determine the layer thicknesses (PPSU and PbSe) that yield maximum absorption at specific target wavelengths. The optimization process iteratively evolves a population of candidate solutions by minimizing reflectance using selection, crossover, and mutation operators. Optimization was performed for each design point from 3 to 5 μm in 0.25 μm steps**,** and the resulting configurations were validated using full-wave FDTD simulations.

To support clarity and reproducibility, Supplementary Table S1 provides a comprehensive summary of the material properties, geometric parameters, and simulation settings used throughout this study. This includes details on the multilayer absorber structure—such as the materials used (graphene, PPSU, PbSe, and gold), wavelength range, optimization strategy, and simulation techniques (TMM and FDTD). Parameters related to electrical switchability, such as the range of

chemical potential values applied to graphene, and the angular range considered for performance analysis, are also included. This table is intended to consolidate all key setup information referenced across the manuscript in a single, accessible format.

**Supplemental Material S2** provides a comprehensive breakdown of the thickness values for each layer in all nine optimized aperiodic multilayer structures presented in this study. These structures, designed to achieve peak absorption at specific wavelengths within the 3–5 μm range (3 μm, 3.25 μm, 3.5 μm, 3.75 μm, 4 μm, 4.25 μm, 4.5 μm, 4.75 μm, and 5 μm), exemplify the precision achievable through our advanced inverse design methodology. The supplemental data outlines the layer-by-layer thicknesses, highlighting how slight variations in thickness enable the systematic tuning of absorption peaks with a resolution of 0.25 μm. This level of detail underscores the importance of precise control over layer dimensions in achieving nearly perfect absorption across the mid-IR atmospheric window, as demonstrated in Figures 3(a) and 3(b) of the manuscript.

Table S1: Detailed dimensions of each layer for the nine optimized structures designed to achieve absorption peaks at specific wavelengths within the mid-IR range (3 μm, 3.25 μm, 3.5 μm, 3.75 μm, 4 μm, 4.25 μm, 4.5 μm, 4.75 μm, and 5 μm).

| | Optimized Wavelength | | | | | | | | |
|---|---|---|---|---|---|---|---|---|---|
| | 3μm | 3.25μm | 3.5μm | 3.75μm | 4μm | 4.25μm | 4.5μm | 4.75μm | 5μm |
| Thickness (nm) | 57.58 | 86.64 | 94.23 | 99.63 | 99.26 | 99.95 | 99.65 | 99.97 | 100 |
| | 258.29 | 488.75 | 485.64 | 322.54 | 487.67 | 305.55 | 398.14 | 488.31 | 462.18 |
| | 0.33 | 0.33 | 0.33 | 0.33 | 0.33 | 0.33 | 0.33 | 0.33 | 0.33 |
| | 293.94 | 477.02 | 26.75 | 97.11 | 165.07 | 311.11 | 317.76 | 268.22 | 455.6 |
| | 0.33 | 0.33 | 0.33 | 0.33 | 0.33 | 0.33 | 0.33 | 0.33 | 0.33 |
| | 339.65 | 108.47 | 29.74 | 323.14 | 128.34 | 165.79 | 49.12 | 32.73 | 39.43 |
| | 0.33 | 0.33 | 0.33 | 0.33 | 0.33 | 0.33 | 0.33 | 0.33 | 0.33 |
| | 56.9 | 30 | 263.67 | 219.76 | 62.17 | 155.33 | 103.81 | 178.83 | 90.88 |
| | 0.33 | 0.33 | 0.33 | 0.33 | 0.33 | 0.33 | 0.33 | 0.33 | 0.33 |
| | 454.4 | 417.91 | 87.65 | 74.61 | 212.1 | 61.57 | 79.04 | 43.74 | 71.98 |
| | 0.33 | 0.33 | 0.33 | 0.33 | 0.33 | 0.33 | 0.33 | 0.33 | 0.33 |
| | 356.52 | 337.26 | 203.12 | 64.44 | 167.94 | 297.17 | 465.53 | 49.28 | 486.23 |
| | 93.87 | 86.61 | 46.86 | 94.11 | 85.68 | 99.85 | 95.36 | 98.55 | 100 |
| Total Thickness (nm) | 1911.15 | 2032.66 | 1237.66 | 1295.34 | 1408.23 | 1496.32 | 1608.41 | 1259.63 | 1806.3 |

Table S2. Rounded thickness values used in the simulation for each optimized structure, along with the corresponding fabrication tolerance range (±5%) applied to the thinnest layer.

| | Optimized Wavelength | | | | | | | | |
|---|---|---|---|---|---|---|---|---|---|
| | 3μm | 3.25μm | 3.5μm | 3.75μm | 4μm | 4.25μm | 4.5μm | 4.75μm | 5μm |
| Thickness (nm) | 58 | 87 | 94 | 100 | 99 | 100 | 100 | 100 | 100 |
| | 258 | 489 | 486 | 323 | 488 | 306 | 398 | 488 | 462 |
| | G | G | G | G | G | G | G | G | G |
| | 294 | 477 | 25 28 | 97 | 165 | 311 | 318 | 268 | 456 |
| | G | G | G | G | G | G | G | G | G |
| | 340 | 108 | 30 | 323 | 128 | 166 | 47 51 | 31 34 | 37 41 |
| | G | G | G | G | G | G | G | G | G |
| | 54 60 | 29 31 | 264 | 220 | 59 65 | 155 | 104 | 179 | 91 |
| | G | G | G | G | G | G | G | G | G |
| | 454 | 418 | 88 | 75 | 212 | 58 65 | 79 | 44 | 72 |
| | G | G | G | G | G | G | G | G | G |
| | 357 | 337 | 203 | 61 68 | 168 | 297 | 466 | 49 | 486 |
| | 94 | 87 | 47 | 94 | 86 | 100 | 95 | 99 | 100 |

**Supplemental Material S3** explores the impact of fabrication errors on the absorption characteristics of the optimized multilayer structure. Fabrication processes inherently introduce variations in layer thickness, with equipment limitations typically resulting in up to a 10% error. To evaluate the robustness of the proposed design, we focused on the thinnest layer, as smaller dimensions are generally more prone to such deviations. This analysis provides crucial insights into the structure's tolerance to fabrication inaccuracies and its reliability in practical applications. Figure S1(a) presents the absorption spectra for the ideal structure (no error) and for structures with ±5% variations in the thickness of the thinnest layer. The results indicate that even with these deviations, the overall absorption spectra remain nearly identical, demonstrating the structure's resilience. Notably, the absorption efficiency remains unaffected, with all structures achieving near-perfect absorption. Figure S1(b) highlights the minimal shifts in the absorption peak due to these errors. The ideal structure, with no thickness deviation, achieves 100% absorption at 3.991 μm. In comparison, a +5% increase in the thinnest layer's thickness shifts the peak to 4.002 μm, while a -5% decrease shifts it to 3.988 μm. These shifts—0.011 μm for +5% and -0.003 μm for -5%—are minimal and well within acceptable ranges for mid-IR applications, showcasing the robustness of the design. Figure S1(c) examines the full width at half maximum (FWHM) of the absorption spectrum across the ideal and error scenarios. The FWHM remains consistent, confirming that the structure's high absorption efficiency and spectral sharpness are unaffected by minor fabrication inaccuracies. This consistency highlights the structure's capability to maintain its designed optical performance despite small deviations in layer thickness.

These results underscore the practicality of the proposed multilayer absorber for real-world manufacturing, demonstrating its ability to sustain high efficiency and precision under fabrication tolerances. By focusing on the thinnest layer, which is most susceptible to errors, we validate the robustness of the entire design, ensuring reliability for advanced mid-IR applications in sensing, imaging, and energy harvesting.

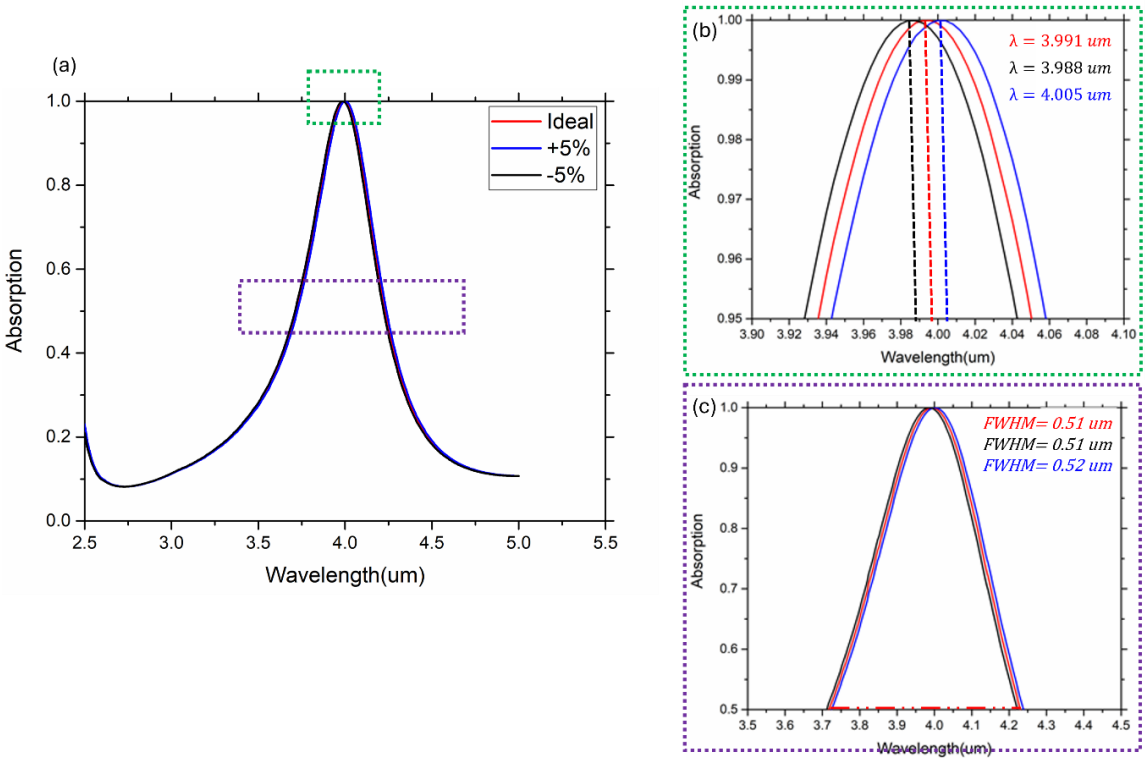


FigS1. (a) Absorption spectra of the ideal multilayer structure and with ±5% fabrication errors in the thickness of the smallest layer, showing negligible changes. (b) Wavelength shift comparison, with 100% absorption at 3.991 µm for the ideal structure, 4.002 µm for +5% error, and 3.988 µm for -5% error. (c) Consistent FWHM across ideal and error conditions, indicating the structure's resilience to thickness variations